Aerodynamic Optimization of Centrifugal Fans Using CFD-Trained Meta-Models

Konrad Bamberger[1]*, Julian Belz[2], Thomas Carolus[1], Oliver Nelles[2]

ISROMAC 2016

International Symposium on Transport Phenomena and Dynamics of Rotating Machinery

Hawaii, Honolulu

April 10-15, 2016

Abstract

Cost-effective optimization of centrifugal fans requires quick and reliable methods to evaluate the target function. A typical target function is maximization of total-to-static efficiency for a given design point. In this work, we suggest to evaluate the target function with CFD-trained meta-models. The meta-models used are artificial neural networks (ANN) and differ from previously developed meta-models in terms of universality since they can be used for optimizing all typical design points of centrifugal fans according to the Cordier diagram.

Since this is the first publication about our research on meta-models for centrifugal impellers, the focus is on methodology. In particular, it is described how an adequate accuracy of the meta-models can be achieved with limited computational resources. For that purpose, the number of simulations required to generate an informative CFD-dataset was reduced by a suitable choice of geometrical parameters and an optimized design of experiments. Reduction of the computational time required for each CFD simulation was achieved by optimizing the computational grid. Eventually, the resulting CFD dataset was efficiently exploited by testing several competing meta-models.

The final meta-models were embedded in an evolutionary optimization algorithm and the resulting geometry was simulated by CFD. The comparison between meta-model prediction and CFD proved the high potential of the methodology since the CFD-predicted efficiency was very high. Nevertheless, it is doubtful if the real aerodynamic optimum was found because the efficiency predicted by the meta-models was even higher and different meta-model types did not yield the same optimal geometrical parameters. For that reason, a plan for future improvements of the meta-models was developed.

.

Keywords

Centrifugal fan — optimization — CFD — meta-model

[1] *Institute for Fluid- and Thermodynamics, University of Siegen, Germany*

[2] *Institute of Mechanics and Control Engineering - Mechatronics, University of Siegen, Germany*

***Corresponding author**: konrad.bamberger@uni-siegen.de

INTRODUCTION

Classic design methods for centrifugal fans are for instance described by Pfleiderer [1, 2] and Bommes [3]. The main advantage of these methods is the low demand for computational resources. However, the strong focus on empirism limits the achievable efficiency and the accuracy with regard to the fulfillment of the design target. For that reason, modern fan design is usually supported by CFD. For instance, the designer can apply the classic methods first, analyze the result by CFD and then try to improve the design based on the interpretation of the CFD results. The full exploitation of the potential for improvement, however, can only be achieved by coupling CFD with optimization algorithms. The main drawback of this method is the associated computational expense. Hence, methods were developed to reduce the required amount of CFD simulations. Ratter et al. [4-6] succeeded to reduce the CFD effort by incorporating preknowledge about the optimal position of the stagnation point at the leading edge. Moreover, a response surface method was used to further reduce the number of required CFD simulations. The response surface method is one example of CFD-trained meta-models which have the advantage that CFD is only required to generate a dataset with which the model is trained. After that, the meta-models predict the fan performance several orders of magnitude faster than CFD.

The present work is also concerned with the development of meta-models and their application in the optimization of centrifugal impellers. The main improvement over previously developed meta-models is their universality since they can be used to aerodynamically optimize centrifugal impellers for all typical design points according to the Cordier diagram. The design point is characterized by the flow rate $\dot{V}$ and the total-to-total pressure rise $\Delta p_{tt} = p_{t2} - p_{t1}$ where the index "t" means total and the indices "1" and "2" refer to positions upstream and downstream of the impeller, respectively. For the sake of comparability, the design point should rather be expressed by the non-dimensional flow and pressure coefficients ϕ and ψ_{tt}:

$$\phi = \frac{\dot{V}}{\frac{\pi^2}{4} D_2^3 n} \tag{1}$$

$$\psi_{tt} = \frac{\Delta p_{tt}}{\frac{\pi^2}{2} D_2^2 n^2 \rho} \tag{2}$$

D_2 is the outer impeller diameter, n is the rotational speed and ρ is the fluid density. Another way to express the non-dimensional design point is to use the specific fan speed σ and the specific fan diameter δ instead of ϕ and ψ_{tt}:

$$\sigma = \frac{n}{\left(2\pi^2\right)^{-1/4} \cdot \left(\frac{\Delta p_{tt}}{\rho}\right)^{3/4} \cdot \dot{V}^{-1/2}} \quad (3)$$

$$\delta = \frac{D_2}{\left(\frac{8}{\pi^2}\right)^{1/4} \cdot \left(\frac{\Delta p_{tt}}{\rho}\right)^{-1/4} \cdot \dot{V}^{1/2}} \quad (4)$$

In many practical applications the kinetic energy of the fluid downstream of the impeller is useless since it dissipates in the surroundings. A definition of the pressure rise which considers the kinetic energy at the impeller outlet as loss is the total-to-static pressure rise Δp_{ts}. The corresponding total-to-static pressure coefficient ψ_{ts} is defined analogously to Equation 2. The efficiency of the impeller is the quotient of air power and the power of the shaft driving the fan:

$$\eta = \frac{\dot{V} \cdot \Delta p}{P_{shaft}} = \frac{\dot{V} \cdot \Delta p}{2 \cdot \pi \cdot n \cdot T_{shaft}} \quad (5)$$

T_{shaft} is the torque of the driving shaft. In principle, the efficiency can be computed with both Δp_{tt} and Δp_{ts}. However, only η_{ts} is relevant for the present work.

The focus of this publication is to demonstrate a computationally cost-effective way to generate the meta-models and to assess their applicability for aerodynamic optimization. The results of the optimizations are planned to be published in future papers.

1. METHODOLOGY

The development of meta-models requires a set of sequential steps that are described in the following. Firstly, the impeller geometry needs to be parameterized (section 1.1). Four representative parameter combinations are picked for validation experiments (1.2). The experimental set-up is described in section 1.3. In order to generate a dataset with which the meta-models are trained, numerous CFD simulations need to be performed. Section 1.4 describes the CFD model. The geometries to be simulated are determined by design of experiments (1.5). For each geometry, the operating point is varied to capture the relevant section of the characteristic curve (1.6). Eventually, the meta-models can be trained with the resulting CFD dataset. An overview about the meta-model outputs is provided in section 1.7. Sections 1.8 and 1.9 describe the general training strategy and specific measures for improving the meta-models, respectively.

1.1 Impeller Parameterization

The main objective of the impeller parameterization is to enable a high level of geometrical flexibility while keeping the number of free geometry parameters to a minimum. For that reason, basic parameters which are also used in classic literature [2, 3] are selected. Those parameters are graphically illustrated in Figure 1 and listed in Table 1. The blades have a circular shape between the inner diameter D_1 and the outer diameter D_2. The hub is a flat disc perpendicular to the axis of rotation. The shroud is not parallel to the hub but tapers between D_1 and D_2. The innermost part of the shroud has a circular shape with the radius r_s. The outer (mostly much larger) part of the shroud has a linear shape determined by the two distances b_1 and b_2 from the hub. The circular arc forming the blade has the constant thickness S. This represents a very simple geometry and thus facilitates cost-effective manufacturing techniques and keeps the number of parameters required to describe the blade shape low. The radius and the centerpoint of the circular arc are given via the inlet angle β_{b1} and the outlet angle β_{b2} which are measured between the circumferential direction and a tangent at the blade leading or trailing edge, respectively. Together with the number of blades z, the aforementioned geometrical parameters are sufficient to describe simple impellers. In order to enable more innovative designs, two more parameters are introduced which are the lean angle δ and the cut-off angle λ. The lean angle δ describes the rotation of the blade around an axis which goes through the centerpoint of the blade section at the hub and which is tangential to the blade at that point. Positive values of δ refer to lean towards the suction side whereas negative values refer to lean towards the pressure side. After applying the lean, it might become necessary to cut material which protrudes beyond the hub/ shroud or the lateral surfaces at D_1/D_2. Accordingly, gaps between the blade and those surfaces are filled maintaining the circular blade shape. The cut-off angle λ is applied to the leading edge of the unwound blade. The two legs of this angle are the original leading edge of the uncut blade and the cut edge which forms the new leading edge. The intersection between those two legs is always at the hub, i.e. the original leading edge position only persists at the hub while material is increasingly cut towards the shroud. Due to lean and cutting the leading edge, the actual blade angles β_{b1} and β_{b2} become variable over the blade height and differ from the original definition used to determine the centerpoint and the radius of the circular arc which forms the blade. Nevertheless, the blade keeps its circular shape which is important to facilitate cheap manufacturing techniques.

From the aforementioned parameters, D_2 and S are not varied by design of experiments but are constant or a function of other geometrical parameters, respectively. The reason for holding D_2 constant is that we consider the dimensionless aerodynamic performance which is independent of D_2. This also applies to the rotational speed n and the fluid density ρ which are held constant, too. The reason why S is no independent parameter is that the blade thickness only has a minor effect on the aerodynamic performance and is usually selected for constructive reasons. We here assume that the blade thickness increases with increasing ratio D_1/ D_2:

$$\frac{S}{D_2} = 0.006 \cdot \sqrt{\frac{D_1}{D_2}} \quad (6)$$

Further geometrical parameters are required to describe the inflow nozzle. Since the inflow nozzle is less relevant with

respect to the aerodynamic performance, those parameters are a function of the impeller parameters and do not need to be varied by design of experiments. The inflow nozzle has a simple geometry and is fully described by its outflow diameter and the radius r_n. All dependent parameters are listed in Table 2.

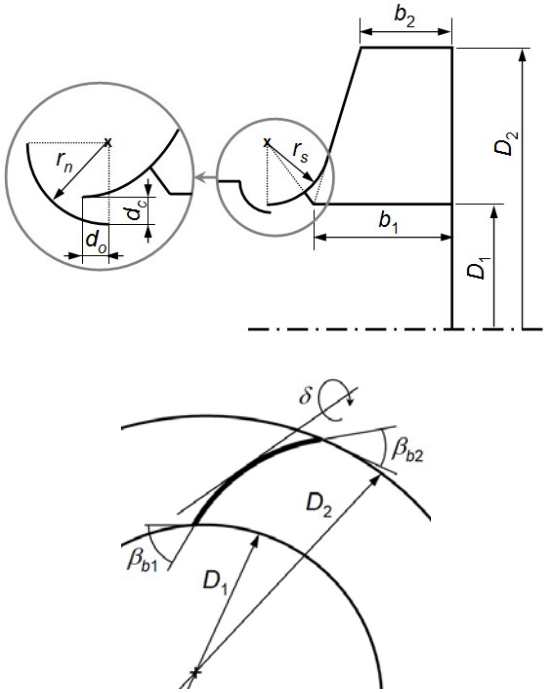

Figure1. Side view and top view of the impeller with indication of the geometrical parameters

Table 1: Independent geometrical parameters

Description	Symbol/ Definition	Min. Value	Max. Value
Number of blades[1]	z	5	16
Diameter ratio	D_1/D_2	0.25	0.8
Inlet blade angle	β_1	20°	60°
Inlet blade angle	β_2	20°	60°
Inlet width ratio[2]	b_1/D_2	0.025	0.4
Outlet width ratio[2]	b_2/D_2	0.025	0.4
Shroud radius ratio	r_s/D_1	0.14	0.3
Lean angle	δ	-15°	15°
Cut-off angle	λ	0°	30°

[1] only integers are possible
[2] b_2 must always be smaller or equal to b_1

Table 2: Dependent and constant geometrical parameters

Description	Symbol/ Definition	Value
Outer diameter	D_2	0.3 m
Rotational speed	n	50 s-1
Fluid density	ρ	1.2 kg/m3
Nozzle radius ratio	r_n/D_1	0.25
Clearance ratio	r_c/D_1	0.02
Overlap ratio	r_o/D_1	0.03

1.2 Impellers for Validation Experiments

Experimental validation of the CFD model is performed with four prototypes which are supposed to be as different as possible regarding both geometry and aerodynamic performance. The geometrical parameters of the first prototype (VAL1) are mostly the mean values of the lower and upper limits indicated by Table 1. The only exception is b_2/D_2 which the mean value of the lower limit and b_1/D_2 of VAL1, i.e. the actual upper limit for the present case taking the constraint $b_2 \le b_1$ into account. At the other three prototypes, all extreme values of the geometrical parameters were used at least once. The allocation of the extremes to the three impellers was performed in such a way that the aerodynamic behavior became as different as possible. For instance, VAL2 is supposed to be associated with high pressure coefficients at small flow coefficients. Hence, the inner diameter and the width are minimal while the number of blades and the exit angle are maximal. VAL3 is supposed to allow for very high flow rates. Consequently, the inner diameter and the width are maximal. VAL4 has no aerodynamic design philosophy but simply contains all extremes of the geometrical parameters that were not used for VAL2 or VAL3. Table 3 summarizes the geometrical parameters of the four impellers.

Table 3: Geometrical parameters of the prototypes

Parameter	VAL1	VAL2	VAL3	VAL4
z	11	16	12	5
D_1/D_2	0.525	0.25	0.8	0.5
β_{b1}	40°	30°	60°	35°
β_{b2}	40°	60°	60°	20°
b_1/D_2	0.213	0.1	0.4	0.2
b_2/D_2	0.119	0.025	0.4	0.1
r_s/D_1	0.22	0.3	0.14	0.2
δ	0°	15°	-15°	15°
λ	15°	30°	0°	30°

1.3 Experimental Set-Up

The four prototypes described in the previous section were built by means of stereolithography and measured on a chamber test rig in accordance with EN ISO 5801 [7]. Figure 2 shows a picture of the test rig and labels the essential components. Air is sucked in through the test rig inflow nozzle at which the static pressure is measured. Given the pressure, the flow rate is calculated with the aid of a calibration curve. The air then passes through a flow straightener, an auxiliary fan and a throttle. The two latter components are required to control the operating point. In the chamber, the air is decelerated. Owing to the large cross-section area, the dynamic pressure in the chamber is negligible and the static pressure measured at the chamber walls is assumed to be equivalent to the total pressure upstream of the fan. The impeller inflow nozzle is integrated in the chamber back wall and aerodynamically connects the test rig with the impeller which is placed behind the chamber. The torque and the rotational speed of the drive motor are measured at the shaft that connects the motor with the impeller. These quantities are required to determine the shaft power and eventually the efficiency.

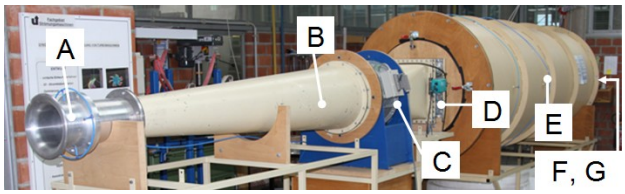

A	Test rig inflow nozzle; measurement of the pressure which eventually yields the flow rate
B	Flow straightener
C	Auxiliary fan
D	Throttle
E	Chamber with flow straightener, measurement of pressure upstream of the test fan
F	Fan stage with inflow nozzle
G	Drive motor, measurement of torque and rotational speed

Figure 2. Chamber test rig in accordance with EN ISO 5801 [7]

1.4 CFD-Model and Optimization of the Grid Resolution

The CFD model used for this work emulates the experimental set-up described in the previous section, i.e. the inflow is assumed to traverse the chamber and the inflow nozzle whereas the outflow area is free of obstacles except for the outer chamber walls. Figure 3 depicts a sketch of all components considered for the CFD-model. The boundary conditions are constant mass flow rate at the inlet, ambient pressure at the opening and no slip at the walls. Hub, shroud and blade are modeled as rotating walls with the rotational speed n whereas all other walls are stationary.

Due to the high number of CFD simulations required to train the meta-models, only stationary simulations were affordable, i.e. the Reynolds-Averaged Navier-Stokes (RANS) method was used. The solver selected was ANSYS CFX 14.5 and the turbulence model used was shear stress transport (SST). As usual in RANS simulations, only one blade channel was simulated and rotational periodicity was assumed at the lateral boundaries. The interface type in between the rotating blade and the stationary environment was frozen rotor.

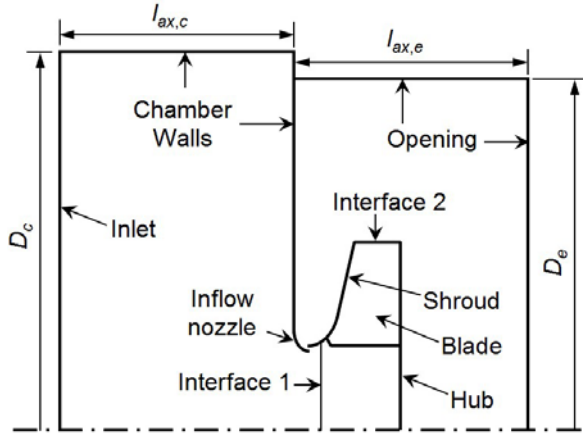

Figure 3. CFD-model

In order to determine the fan performance data described in the introduction, the quantities Δp_{ts}, Δp_{tt} and T_{shaft} must be extracted from the CFD results. Δp_{ts} is the difference between the area-averaged pressure at the opening and the inlet. The dynamic pressure required to determine Δp_{tt} was evaluated at the interface between the impeller outlet and the environment. The overall shaft torque T_{shaft} equals the sum of the torques at all rotating surfaces, i.e. the surfaces at the blade, the hub and the shroud.

The computational grid of the impeller was generated with ANSYS TurboGrid 14.5 and the grid of the environment was generated with ICEM CFD. A grid optimization was performed to find the best compromise between accuracy on the one hand and numerical cheapness on the other hand. The accuracy was estimated by comparing the numerical results with the experimental results of the prototypes in terms of ψ_{ts} and η_{ts}. This comparison was performed for the prototypes VAL1, VAL2 and VAL4. Three operating points were considered for each impeller to cover the operational conditions of partial load, maximum η_{ts} and overload. VAL3 was excluded from the optimization since its aerodynamic behavior is extremely instationary and impossible to be predicted by RANS simulations independent from the grid resolution. Section 2.2 discussed in more detail how to deal with problematic impellers such as VAL3. The high number of 18 quantities to be compared (ψ_{ts} and η_{ts} at three impellers with three operating points each) is important to mitigate the dependency of the target function on random effects. The numerical expense of a simulation was considered by a penalty term which is a function of the overall number of nodes N. It is defined such that 500,000 extra-nodes should reduce the averaged difference between CFD and experiment by at least 0.01. Otherwise, an increase of nodes impairs the target function. The mathematical definition of the target function is provided by Equation 7:

$$F = \frac{1}{18}\sum_{i=1}^{9}\left(\left|\psi_{ts,CFD,i} - \psi_{ts,exp,i}\right| + \left|\eta_{ts,CFD,i} - \eta_{ts,exp,i}\right|\right) + 0.01 \cdot \frac{N}{5 \cdot 10^5} \tag{7}$$

Besides the overall number of nodes N, the distribution of the nodes has an essential effect on the target function. For instance, one optimization parameter was defined to control the ratio between the number of nodes in the grid around the impeller and the number of nodes in grid of the environment. Further optimization parameters were introduced to control the distribution of nodes within each of the grids. At the impeller grid, an additional optimization parameter was required to balance the resolution in axial direction against the resolution in meridional direction. Moreover, two parameters were introduced which determined the intensity of the typical grid refinement in the boundary layers at both impeller and environment. Eventually, the size of the environment also has an impact on the target function. On the one hand, its dimensions must be large enough to avoid an unphysical impact of the boundary conditions on the fan performance. On the other hand, too large dimensions at a given overall number of nodes increases the cell sizes and hence reduce the numerical accu-

racy. The dimensions that were varied are indicated in Figure 2, i.e. the axial length of the chamber ($l_{ax,c}$) as well as the axial length and the diameter of the volume around the impeller ($l_{ax,e}$ and D_e). The diameter of the chamber is not varied since it is equal to the experimental set-up ($3.7 \cdot D_2$). Altogether there were eight grid parameters to be optimized. This was performed using the Simplex method by Nelder and Mead [8].

1.5 Design of Experiments

One crucial step in building a meta-model is the design of experiments (DoE). It determines which geometric parameter combinations should be investigated by CFD simulations. As recommended by Santner et al. [9], a space filling design should be chosen, if no prior knowledge about the process is available. Due to its advantages and simplicity [9] a latin hypercube (LH) design has been used. The non-collapsing property of LH designs is one advantage compared to commonly used grid designs. Non-collapsing means, that if all data points are projected onto one axis, all values along that axis only occur once. In order to achieve good space filling properties the LH design was optimized with the extended deterministic local search method described by Ebert et al. [10].

Due to the time restrictions it should be possible to simulate about 2000 different geometries. The question arises, if in addition to an LH design all corners of the input space should be simulated. For the nine dimensional input space this would be about 25% (2^9 = 512) of all data points. The positive effect assumed is the lower demand for extrapolation. Expecting that the demand for extrapolation is of minor importance and considering the results from Belz et al. [11], it was decided to not simulate all possible corners.

Once the optimization of the LH design is finished, the order in which the geometries are simulated needs to be defined. The goal of a specific order is to obtain models that capture the behavior of almost all geometries as good as possible at any time. Therefore the already measured geometries should cover the input space as uniformly as possible while being as space filling as possible. To achieve this goal, all data points of the optimized LH design were clustered using the intelligent *k*-means algorithm (see Mirkin [12]). Basically this algorithm incorporates the classic k-means algorithm, but the number of clusters *k* is determined automatically, see Mirkin [12] for more details. Once each data point was assigned to one cluster, the data points within each cluster were ordered. Starting with the point next to the cluster center, the next points were chosen such that distances between the already ordered points were as large as possible. After that the ordering algorithm went from cluster to cluster and picked the first remaining element from each ordered cluster list and added it to the overall ordering list, leading to the final measurement order. Because each cluster represents another area of the input space, this procedure should guarantee to have points from all areas as early as possible.

1.6 CFD-Simulation of the DoE

Points of the Characteristic Curve to be Simulated

The section of the characteristic curve that is relevant to the present work is the operating range between zero flow rate (ϕ = 0) and zero total-to-static pressure rise (ψ_{ts} = 0). To save computational time, each new simulation was initialized with the previous one. The first point of a characteristic curve that was simulated was always the estimated flow coefficient where ψ_{ts} becomes zero. At the beginning of the project this point had to be estimated by theoretical models [13]. After approximately 200 geometry variations, however, it was estimated more precisely by preliminary meta-models. From that operating point onwards, the flow coefficient was reduced in seven steps. After that, the density of operating points was enhanced in two important areas of the characteristic curve if required. One of them was the operating area with highest η_{ts}. The flow coefficient where η_{ts} becomes maximal was interpolated based on the existing CFD results and an additional CFD simulation was performed if it differed by more than $\Delta\phi$ = 0.003 from the existing curve points. The same strategy was applied to the operating point of zero ψ_{ts} to check if the initial estimation was sufficiently precise.

Time Step Control

As mentioned previously, the RANS equations were solved with ANSYS CFX. One essential parameter that influences the convergence is the time scale. For the present work, the "physical time scale" option was selected. In general, large magnitudes of the time scale on the one hand often accelerate the rate of convergence but on the other hand also favor divergence and numerical overflow. Unfortunately, the optimal time scale is individual for each simulation and cannot be estimated in advance. For that reason, the present work used an adaptive choice of the time scale. The starting value for the first simulation of one fan geometry was always very low (0.0005 s). This time scale was, however, only used to guarantee stability in the first 50 iterations. After that, it was multiplied by 10 (i.e. 0.005 s). Potential numerical instability due to a too large time scale was detected based on the residuals and on the fluctuation of integral quantities (e.g. ψ or η) over the iterations. In case of high residuals or high fluctuations of the integral quantities, the time scale was decreased until numerical stability was restored.

1.7 Strategies to Predict the Characteristic Curves by Meta-Models

There are basically two ways to predict characteristic fan curves. The simplest approach is a direct prediction of the quantities of interest (e.g. ψ or η). The disadvantage of that strategy is that these quantities are dependent on the flow coefficient which therefore has to be considered as an additional input to the meta-models. This not only increases training time, but also increases the complexity of the meta-models which eventually increases the risk of overfitting effects.

An alternative is to use parameterized shapes of the characteristic curves. In that case, the meta-models are used to pre-

dict the curve parameters and the characteristic curve is built on the basis of these curve parameters. One essential advantage of that method is that the curve parameters are only dependent on the impeller geometry. As a consequence, ϕ is no meta-model input. Another advantage of this method is that the curve parameters can be physically interpretable quantities such as the flow coefficient at zero ψ_{ts} or maximum η_{ts}. This allows direct control over the most important points of the characteristic curve. The main disadvantage of this method is the loss of flexibility since not all curve shapes can be emulated by the pre-defined functions in an adequate way. A further problem is the accumulation of errors if more than one curve parameter is predicted imprecisely. Unfortunately, the two disadvantages mentioned require conflicting measures for mitigation. Higher flexibility can, for instance, be achieved by a higher number of curve parameters which, however, amplifies the accumulation of errors. Hence, an adequate solution must incorporate as much prior knowledge as possible such that most curves can be emulated adequately with only a few curve parameters.

It was found that knowledge about only two operating points enables an adequate prediction of the $\psi_{ts}(\phi)$ curve. Those two operating points are the zero-crossing ($\phi_{\psi ts=0}$) and the operating point where the product of ϕ and ψ_{ts} (i.e. the power coefficient $\lambda_{ts}(\phi)$) becomes maximal. The latter operating point actually contains two important pieces of information: (i) a further operating point on the $\psi_{ts}(\phi)$ curve ($\psi_{ts} = \lambda_{ts} / \phi$) and (ii) the first derivative ($\psi'_{ts} = -\psi_{ts} / \phi$, assuming that λ'_{ts} is zero at that operating point). Given these three pieces of information, the full $\psi_{ts}(\phi)$ curve can be built up by a second degree polynomial.

The typical curve shape of $\eta_{ts}(\phi)$ is more complex than the curve shape of $\psi_{ts}(\phi)$ and hence cannot be modeled adequately by a second degree polynomial. Instead, the Equations 8 and 9 were used. These equations contain the important operating point of maximum η_{ts} (i.e. $\eta_{ts,max}$ and $\phi_{\eta ts,max}$). From that operating point onwards, $\eta_{ts}(\phi)$ is assumed to decay in both directions. On the left hand side, the curve crosses zero at $\phi = 0$. On the right hand side, the flow coefficient where η_{ts} becomes zero is identical with the flow coefficient that was already required to determine the zero-crossing of $\psi_{ts}(\phi)$, i.e. $\phi_{\psi ts=0}$. The curvature between the maximum and the zero-crossings is controlled by the exponents $p_{\eta 1/2}$ which are defined individually for each side.

$$\eta_{ts}(\phi) = \eta_{ts,max} - \frac{\eta_{ts,max}}{\phi_{\eta ts,max}^{p_{\eta 1}}} \cdot \left(\phi_{\eta ts,max} - \phi\right)^{p_{\eta 1}} \quad (8)$$

(for $\phi \le \phi_{\eta ts,max}$)

$$\eta_{ts}(\phi) = \eta_{ts,max} - \frac{\eta_{ts,max}}{\left(\phi_{\psi ts=0} - \phi_{\eta ts,max}\right)^{p_{\eta 2}}} \cdot \left(\phi - \phi_{\eta ts,max}\right)^{p_{\eta 2}} \quad (9)$$

(for $\phi \ge \phi_{\eta ts,max}$)

The curve parameters were determined for all characteristic curves that were simulated using the Simplex optimization method. The target function was the minimum averaged difference between the CFD results and the modeled curve.

1.8 Training of the Meta-Models

Two meta-model types were tested: Local Model Networks (LMN) and Multi-Layer Perceptrons (MLP).

LMNs follow a divide-and-conquer strategy. The input space spanned by all geometry parameters is divided into small sub-spaces, where simple local models are able to sufficiently well describe a part of the whole function to be approximated. The local models are interpolated in between two adjacent sub-spaces. The structural complexity of a LMN is directly related to the number of sub-spaces and the architecture of the local models. The identification of the sub-spaces, i.e. the shape, the location and the number of sub-spaces, as well as the determination of the local model parameters is part of the so-called training. For the training of the LMNs the hierarchical local model tree (HILOMOT) algorithm (see Nelles [14]) was used with local linear models. The structure of the LMN grows incrementally by adding a further division of one pre-existing sub-space. Therefore, one local model is added in each step until a termination condition is met. For the determination of the shape and location of the sub-space to be added, a nonlinear optimization is necessary. The parameter determination of the local linear models can be carried out via least squares. In the HILOMOT algorithm the least squares problem is nested in the nonlinear optimization for the partitioning, leading to a separable nonlinear least squares problem (see Nielsen [15]) with excellent convergence properties. With each added local model, the flexibility and thereby the ability to describe more complex processes of the LMN is increased. The user has to avoid too flexible models, since at some point the LMN is able to describe random deviations that do not originate from the true process behavior like e.g. noise. This effect is well known as overfitting. For the automatic prevention of overfitting the available data can be split into two data sets for training and validation. Two types of errors follow from the data splitting, the training and the validation error. The minimization of the training error through the model parameter tuning is done without any information about the validation error. The latter is only utilized to test the generalization ability of the model. An increase of the validation error indicates beginning overfitting. For the termination of the LMN training process 20% of the available data was utilized as validation data. As soon as the validation error increased two times in succession, the training was terminated in order to prevent the model from overfitting

MLPs consist of the input layer, one or more hidden layer(s) and the output layer. The number of hidden layers and the number of neurons in each of the hidden layers determines the complexity of the model. In the present work, two hidden layers were used and the number of neurons in each hidden layer was optimized. The optimization problem was initialized by training an MLP with only two neurons in each hidden layer. Afterwards, the number of neurons in each hidden layer could be increased or decreased by one leading to eight possible structures (1 layer - 1 layer, 1-2, 1-3, 2-1, 2-3, 3-1, 3-2 and 3-3). MLPs were trained for all of these structures

and the MLP with the lowest validation error was selected as the interim optimum from where the procedure of testing all surrounding structures was repeated. The structure optimization was stopped when none of the structure changes led to a decrease in the validation error. Training an MLP for a given structure means optimization of the weights in the hidden layers. This was performed with the Neural Network Toolbox of Matlab which uses the Levenberg-Marquardt method. The target function of the weight optimization was the mean squared difference between the MLP output and the CFD results. 80% of the available CFD data was used for that purpose whereas the remaining 20% was used for validation. The training process was terminated prematurely if the validation error increased six times in succession which is assumed to indicate overfitting. Eventually, the training state with the minimal validation error was selected. Since the Levenberg-Marquardt method is a local optimization algorithm, the result depends on the initialization. For that reason, the weight optimization of each structure to be tested was performed with twelve different initializations and only the MLP with the lowest validation error was used for the comparison with other structures.

1.9 Further Measures to Improve the Meta-Model Performance

One simple possibility to improve the meta-model performance was pursued here. It is based on improving the bias-variance tradeoff by input selection. Only inputs advantageous to the overall performance shall be included in the meta-model. This input selection was performed by backward elimination. Backward elimination is a search strategy that starts with a full model and removes the least significant inputs step by step. In contrast to the opposite approach called forward selection this strategy takes correlations between the (potential) inputs into account at the price of higher computational effort.

Once an input is removed, it can not be added afterwards. Since the meta-model inputs correspond to the centrifugal fan geometry parameters, which are carefully chosen according to expert knowledge, it seems not reasonable to neglect some of them. However, especially in early stages where only a small amount of data is available, the concentration on the most important inputs might be beneficial. Loosely speaking, the uncertainty of the meta-model parameters is high, if the number of samples is small. Decreasing the number of inputs goes along with less parameters in the model, such that for the estimation of each remaining parameter in relative terms more information is available. Lowering the parameter uncertainty of the model can overcompensate the loss of information due to discarded inputs, such that the model generalization performance increases. This phenomenon is well known as bias-variance tradeoff, see Bishop [16] for more information.

2. RESULTS

All of the results presented in the following are based on a dataset of 622 simulated characteristic fan curves. The dataset is growing continuously which is likely to enhance the results in the future. The results that heavily depend on the size of the CFD dataset comprise the quality of the meta-models (section 2.2), the range of design points that could be realized so far (2.3) and the suitability of the meta-models to be used in optimization algorithms (2.5).

2.1 Optimal Computational Grid

Given the penalty term which accounts for computational effort, the ideal overall number of nodes is approx. 650,000. 77% of the nodes should be used to mesh the blade channel whereas only 23% should be used to mesh the environment. The optimal balance between the resolution of the boundary layers and the resolution of other regions leads to an averaged dimensionless wall distance of $y^+ \approx 12$ at the impeller surfaces and $y^+ \approx 18$ at surfaces in the environment. Naturally, the non-averaged local magnitudes can differ significantly depending on the location on the surface, the blade geometry and the operating point. The optimal balance between the resolution in axial and in meridional direction is achieved by similar cell sizes in either direction.

The optimal dimensions of the environment ($l_{ax,c}$, $l_{ax,e}$ and D_e) were found to be very weak optimization parameters if critical magnitudes are exceeded. Therefore, it was possible to slightly modify these dimensions with only a minor impact on the predicted performance. It was decided to adapt the two axial lengths to one fan diameter ($l_{ax,c} = l_{ax,e} = D_2$) and to adapt the diameter of the environment to the diameter of the chamber ($D_e = D_c = 3.7D_2$).

All CFD results presented in the following are based on computational grids generated with the optimal grid parameters listed above.

2.2 Quality of the CFD Model

Figure 4 compares the CFD-simulated and measured characteristic curves of three validation examples in terms of ψ_{ts} and η_{ts}. Not all CFD-simulated operating points are depicted since some results are considered unreliable. This applies to all operating points with strong secondary flows and a highly instationary flow field which cannot be computed adequately with the RANS equations. Two criteria are defined to detect unreliable CFD results. The first criterion deals with the wall shear stress τ_w at the blade. Magnitudes smaller than 1 Pa generally indicated flow separation. The four validation examples showed that the difference between CFD and experiment becomes significant if the area-averaged wall shear stress falls below a critical magnitude. When computing the average, all areas with attached flow ($\tau_w \geq 1$ Pa) were weighted with $\tau_w = 1$ Pa to avoid that very high local magnitudes bias the conclusion. Equation 10 states the mathematical formulation in which the index i represents the cell number of the computational grid on the blade surface and G is the overall number of cells on the blade surface.

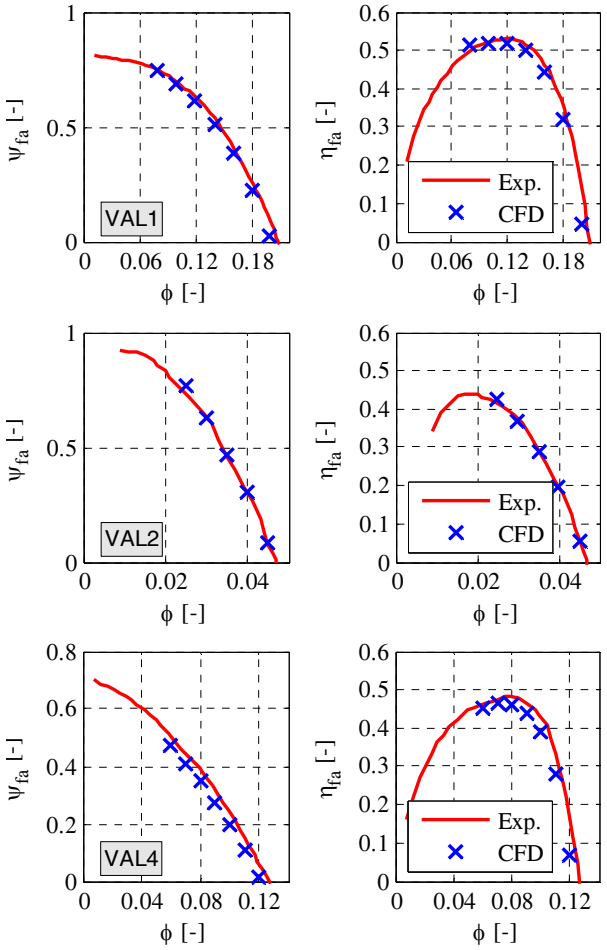

Figure 4. Comparison between CFD and experiment for VAL1, VAL2 and VAL4

$$\overline{\tau}_w = \frac{1}{A_{blade}} \sum_{i=1}^{G} \min\{\tau_i, 1\,\text{Pa}\} \cdot A_i \qquad (10)$$

The second criterion deals with radial backflow in the blade channel. In an ideal flow field, there is only flow from the inside to the outside. Secondary flows, however, can lead to local backflow. The intensity of backflow is measured by the quotient of two differently computed mass flow rates in radial direction. In the denominator, the sign of the local mass flow rate is taken into account to the effect that the positive and negative parts of circulating flow cancel out. In the numerator, only the absolute value of the local mass flow rate is considered to the effect that circulating flow increases the sum. The formula for the quotient x_{mr} is stated in Equation 11. The index i is the cell number and H is the number of cells in the volume between D_1 and D_2.

$$x_{\dot{m}_r} = \frac{\sum_{i=1}^{H} |\dot{m}_{r,i}|}{\sum_{i=1}^{H} \dot{m}_{r,i}} \qquad (11)$$

Significant discrepancies between CFD and experiment were observed for τ_w < 0.7 Pa or x_{cr} > 1.1. As it can be observed in Figure 4, the agreement between CFD and experiment is very good for operating points which do not violate the two criteria for instationary flow. It is hence concluded that the CFD model is suitable to compute the performance of fans with a decent flow field and to detect operating points with strong secondary flows. Since optimized fans are unlikely to be associated with strong secondary flows, the CFD model appears to be suitable for optimization purposes, too.

The operating points sorted out in the four validation examples comprise the operating area of strong partial load in case of VAL1, VAL2 and VAL4 but the complete characteristic curve of VAL3.

2.3 Achievable Design Points

It is commonly agreed that not all design points can be realized with centrifugal fans. Cordier [17] found that there is a correlation between the specific fan speed σ and the specific fan diameter δ which limits the achievable design points to a narrow band in the σ-δ diagram. Moreover, not all specific fan speeds are suitable for centrifugal fans. Carolus [13] presents a σ-δ diagram in which the classic realm of centrifugal fans is assumed to be in the range $0.1 \le \sigma \le 0.5$. Smaller magnitudes are typically realized by displacement machines, larger magnitudes are typically realized by mixed-flow or axial fans.

Figure 5 depicts a σ-δ diagram in which the typical correlation between σ and δ is illustrated by a black curve based on a formula by Pelz [18]. The grey area represents the range of the operating points that were simulated in the context of the DoE. It can be observed that this area forms a band around the curve suggested by Pelz in the range $0.07 \le \sigma \le 2$. Hence, it is confirmed all typical design points of centrifugal fans can be realized with the present input space. In fact, the design space is even extended since much smaller or larger specific fan speeds than usually used for centrifugal fans can be realized, too. In contrast, an extension of the design space towards unusually small or large specific fan diameters for a given specific fan speed cannot be observed. This might be realized by applying the meta-models in optimization algorithms targeting at the realization of extraordinary design points which is planned in the near future.

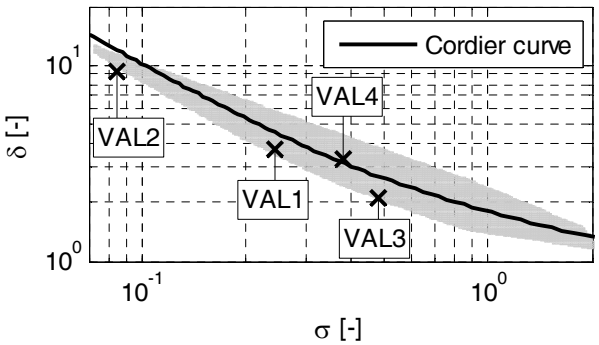

Figure 5. Cordier diagram with indication of all operating points simulated so far (grey area).

2.4 Comparison of Different Meta-Model Approaches

As mentioned previously, two different model types were tested which are the LMN and the MLP. Moreover, two differ-

ent approaches to predict the characteristic fan curves were presented, i.e. the direct prediction of ψ_{ts} and η_{ts} using ϕ as an input and the prediction of curve parameters that only depend on the impeller geometry. Regarding the second approach, it is either possible to predict all curve parameters by a single meta-model or to use an individual meta-model for each curve parameter. Altogether, these options lead to six different approaches of how to predict the impeller performance by meta-models. The assessment of an approach cannot be based on the validation error since this would favor the MLPs over the LMNs. The reason is that the validation error is much more involved in the training of MLPs as compared to LMNs. It is used as the target function of the structure optimization of the MLPs and to select the best MLP after testing numerous different weight initializations. As a consequence, the validation error of the final MLP might benefit from random effects. An objective comparison is only feasible using a test dataset which by no means was involved in the training method. The test data used here consists of the 150 most recent geometry variations which are not part of the aforementioned 622 geometries used for training and validation. The test error was computed as the root mean squared error (RMSE) between all CFD results of the test data and the corresponding meta-model predictions. Operating points violating at least one of the two criteria for instationary flow were not considered.

Table 4 lists the RMSE of all six approaches. Although the MLP approach with individual prediction of the curve parameters currently works best regarding both ψ_{ts} and η_{ts}, it is too early to draw a final conclusion because the difference to other approaches is small. Moreover, there is neither a universal tendency regarding the choice between LMN or MLP nor regarding the choice between the distinct approaches to model the characteristic curves. It is planned to observe the development of the ranking as the available CFD data increases. This will reveal to which extent the present ranking is biased by random effects.

Table 4: Meta-Model approaches ranked by the test error

ψ_{ts}			η_{ts}		
Rank	Type[1]	RMSE	Rank	Type[1]	RMSE
1	MLP-ind	0.052	1	MLP-ind	0.052
2	LMN-col	0.055	2	MLP-unmod	0.057
3	MLP-col	0.062	3	LMN-ind	0.059
4	LMN-unmod	0.063	4	LMN-col	0.059
5	LMN-ind	0.066	5	MLP-col	0.062
6	MLP-unmod	0.077	6	LMN-unmod	0.064

[1] ind/col = modeled characteristic curve with individual/ collective prediction of the curve parameters
unmod = unmodeled characteristic curve

2.5 Suitability of the Meta-Models for Optimization

Meta-model of very high quality are required if they are to be used to evaluate the target function in optimization algorithms. The reason is that any weak point of the meta-model (where the predicted efficiency is unrealistically high) will be exploited by the optimization algorithm instead of finding the real aerodynamic optimum. The assessment if the present meta-models are suitable for optimization was performed by conducting unconstrained optimizations with the target of maximum η_{ts}. The resulting geometries were then simulated by means of CFD and the CFD results were compared to the meta-model prediction. An evolutionary optimization was used. The implementation is an in-house Matlab code which was inspired by the work by Thévenin and Janiga [19]. The number of individuals per generation was 1000. The generation of an offspring generation was mostly conducted with the "crossover" method and only a small portion of the offspring generation was based on the "averaging" method. Moderate and random mutation was applied after the generation of the offspring. Given these settings, the algorithm converged after a couple of hundred generations and yielded repeatable results that were independent of the initialization of the first generation. The algorithm was run two times predicting $\eta_{ts,max}$ with the LMN-ind or MLP-ind method, respectively.

The resulting geometries are similar in many respects, e.g. a middle-sized inner diameter, flat inflow and outflow angles, large shroud radii and negative lean. However, there are also differences which indicate that at least one design (but most probably both of them) are not aerodynamically optimal. CFD simulations revealed that the geometry suggested by the LMN has a slightly higher efficiency. Nevertheless, also the LMN optimization was only partly successful. On the one hand, it led to a total-to-static efficiency as high as 63 % which exceeds the efficiency of all operating points simulated in the context of the DoE. On the other hand, the MLP prediction of η_{ts} was still considerably higher (67 %) wherefore it is assumed that the optimization result is still biased by weaknesses of the meta-model. For that reason, the optimal geometries are not discussed in detail and no characteristic curves are presented in the present publication. Making the meta-models suitable for optimization problems is the highest priority in the ongoing research.

3. CONCLUSIONS

A promising methodology to train CFD-based meta-models for centrifugal impellers was demonstrated. It was shown that the selected geometrical input space is sufficient to design impellers for the complete classic realm of centrifugal fans according to the Cordier diagram. Due to an optimized DoE and an optimized order in which the DoE was simulated, meta-models with satisfactory performance were obtained after only 622 CFD-simulated geometry variations. This is a small number in view of a nine-dimensional input space and wide ranges between the minimum and maximum value of each parameter. The computational cost to generate the CFD dataset was reduced by optimizing the computational grid with the target of finding the best compromise between accuracy and computational cheapness. Experimental validation with four prototypes proved that sufficient accuracy can be achieved with 650,000 nodes if the distribution of the nodes within the grid is optimal. In addition, computational cost was reduced by an adaptive selection of the time scale and the operating points to be simulated.

The main drawback of the methodology was encountered when coupling the meta-models with optimization algorithms targeting at maximum η_{ts}. It was observed that different meta-model types lead to different optimization results and that the actual performance of the resulting geometry differs from the meta-model prediction. Nevertheless, the efficiency of the optimized design was still higher than any other efficiency obtained during the simulation of the DoE which proves the high potential of the methodology.

In order to obtain better results in the future, a larger CFD dataset is required. A total of 2138 curve simulations are sought based on DoE. Afterwards, a so-called active learning phase will follow. The basic idea is to exploit information from the already simulated points with the help of meta-models based on the available data. This procedure is called hierarchical local model tree for design of experiments (HILOMOTDoE) and tries to find locations in the input space where the most information gain can be expected by discovering regions where the current meta-model performs worst. See Hartmann et al. [20] for more detailed information.

Once the accuracy of the meta-models is good enough for application in aerodynamic optimization problems, it is planned to seek for the same findings as recently obtained with meta-models for axial impellers. These findings comprise the estimation of the achievable total-to-static efficiency as a function of the design point [21], design guidelines for the optimal choice of geometrical parameters as a function of the design point [22] and aerodynamic explanations for the enhanced performance [23].

ACKNOWLEDGMENTS

This work was funded by the German Ministry for Economic Affairs and Energy (BMWi), the German Federation of Industrial Research Associations (AiF) and the Research Association for Air and Drying Technology (FLT).

REFERENCES

[1] Pfleiderer, C., 1961, Die Kreiselpumpe für Flüssigkeiten und Gase, *Springer Verlag*, Berlin-Heidelberg.

[2] Pfleiderer, C., Petermann, H., 1991, Strömungsmaschinen, *Springer-Verlag*, Berlin, Germany.

[3] Bommes, L., Fricke, J., Grundmann, R., 2003, Ventilatoren, *Vulkan Verlag*, Essen.

[4] Ratter, H., Caglar, S., Gabi, M., 2012, "A Combination of Conventional Layout Desing and Numerical Methods for the Optimization of Centrifugal Fans", *Proc. 14th International Symposium on Transport Phenomena and Dynamics of Rotating Machinery, ISROMAC-14*, Honolulu, Hawaii, USA.

[5] Ratter, H., Çağlar, Ş., Gabi, M., 2013, "Empirical model for the quantitative prediction of losses of radial fans based on CFD calculations", *Proc. 11th International Symposium on Experimental and Computational Aerothermodynamics of Internal Flows,* Shenzhen, China.

[6] Ratter, H., Çağlar, Ş., Gabi, M., 2014, "A Coupled Blade Adjustment and Response Surface Method for the Optimization of Radial Fans Without Housing", *Proc. ASME TurboExpo 2014,* Düsseldorf, Germany.

[7] EN ISO 5801:2009, 2010, "Industrial Fans - Performance Testing Using Standadized Airways," *Beuth Verlag, Berlin, Germany*, Berlin, Germany.

[8] Nelder, J. A., Mead, R., 1965, "A Simplex Method for Function Minimization", *Computer Journal*, 7, pp. 308-313.

[9] Santner, T., Williams, B., Notz., W., 2003, The design and analysis of computer experiments, *Springer Science & Business Media*.

[10] Ebert, T., Fischer, T., Belz, J., Heinz, T. O., Kampmann, G., Nelles, O., 2015, "Extended Deterministic Local Search Algorithm for Maximin Latin Hypercube Designs", *Proc. IEEE Symposium on Computational Intelligence in Control and Automation*.

[11] Belz, J., Nelles, O., 2015, "Proposal for a Function Generator and Extrapolation Analysis", *Proc. International Symposium on Innovations in Intelligent Systems and Applications*.

[12] Mirkin, B., 2005, "Clustering for Data Mining: A Data Recovery Approach", *Chapmann and Hall/CRC*.

[13] Carolus, T., 2012, Ventilatoren - Aerodynamischer Entwurf, Schallvorhersage, Konstruktion, *Springer Vieweg*, Wiesbaden, Germany.

[14] Nelles, O., 2006, "Axes-Oblique Partitioning Strategies for Local Model Networks", *Proc. International Symposium on Intelligent Control*.

[15] Nielsen, H. B., 2000, "Separable Nonlinear Least Squares",Lyngby, Tech. Rep.

[16] Bishop, C. M., 1995, Neural Networks for Pattern Recognition, *Clarendon Press*, Oxford, UK.

[17] Cordier, O., 1953, "Ähnlichkeitsbedingungen für Strömungsmaschinen", *BWK*, 5(10), pp. 337-340.

[18] Pelz, P., Metzler, M., 2012, "Optimization of Power-Specific Investment Costs for Small Hydropower", *Proc. 17th international Seminar on Hydropower Plants*.

[19] Thévenin, D., Janiga, G., 2008, Optimization and Computational Fluid Dynamics, *Springer Verlag GmbH*, Heidelberg, Germany.

[20] Hartmann, B., Ebert, T., Nelles, O., 2011, "Model-based Design of Experiments Based on Local Model Networks for Nonlinear Processes with low Noise Levels", *Proc. American Control Conference*.

[21] Bamberger, K., Carolus, T., 2015, "Achievable Total-to-Static Efficiencies of Low-Pressure Axial Fans", *Proc. International Conference on Fan Noise, Technology and Numerical Methods,* Lyon, France.

[22] Bamberger, K., Carolus, T., 2015, "Design Guidelines for Low Pressure Axial Fans Based on CFD-Trained Meta-Models", *Proc. European Turbomachinery Conference 11,* Madrid, Spain.

[23] Bamberger, K., Carolus, T., 2015, "Analysis of the Flow Field in Optimized Axial Fans", *Proc. ASME TurboExpo,* Montreal, Canada.